ACS Catalysis

pubs.acs.org/acscatalysis Research Article

Direct Evidence of the Role of Co or Pt, Co Single-Atom Promoters on the Performance of MoS_2 Nanoclusters for the Hydrogen Evolution Reaction

Luz A. Zavala, Kavita Kumar, Vincent Martin, Frédéric Maillard, Françoise Maugé, Xavier Portier, Laetitia Oliviero,* and Laetitia Dubau*

Cite This: *ACS Catal.* 2023, 13, 1221−1229 Read Online

ACCESS | Metrics & More | Article Recommendations | Supporting Information

ABSTRACT: Developing alternatives to platinum (Pt) and iridium (Ir) in proton-exchange membrane water electrolyzers is crucial on the way to viable energy provision schemes. However, although it seems difficult to substitute Ir, alternatives exist for Pt at the proton-exchange membrane water electrolyzer cathode. Here, we report on the synthesis and the characterization of efficient and durable hydrogen evolution reaction (HER) nanocatalysts based on MoS_2 supported on high-surface-area carbon. Citric acid was used as a chelating agent to control the size of the MoS_2 crystallites (1.4 nm) and thus the density of active sites (slab edges). Inspired by successful approaches in catalysis for hydrodesulfurization reactions, conventional 2H MoS_2 was sequentially doped with cobalt (Co) and then with 1 wt % of Pt. Overpotentials of 188, 140, and 118 mV at 10 mA cm^{-2} are reported for MoS_2/C, Co−MoS_2/C, and $Pt_{1\%}$−$CoMoS_2$/C, respectively. This result is attributed to the weakening of the H_{ads} binding energy of the promoted MoS_2-edge active sites (because the promoting atoms are mostly located at the edges). Associated with small-metal dissolution rates (monitored in situ, during the HER), our findings demonstrate that metal promotion (doping) is a promising route to replace Pt with earth-abundant elements in acidic water electrolyzers.

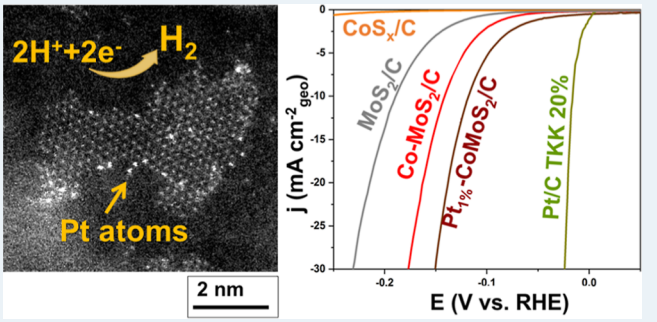

KEYWORDS: *proton-exchange membrane water electrolyzer (PEMWE), non-noble electrocatalyst, hydrogen evolution reaction (HER), single-atom-promoted molybdenum sulfides, durability*

1. INTRODUCTION

The deleterious effects of greenhouse gases on the earth's climate trigger an intensive search for environmentally friendly alternative energy resources.[1] In that frame, renewable energies are promising candidates, but large-scale energy storage systems are required to counterbalance their intermittency. Electrochemical and photoelectrochemical water electrolyzers are best suited to use the surplus of electrical energy produced from renewables and produce molecular hydrogen (H_2), an energy vector with high energy density and minimal environmental impact. However, at the moment, only proton-exchange membrane water electrolyzers (PEMWEs) can withstand the rapid and large-amplitude variations of power induced by wind turbines or solar photovoltaics. Platinum (Pt) nanoparticles in the range of 2−3 nm supported on high-surface carbon are the benchmark catalysts to electrocatalyze the hydrogen evolution reaction (HER) at PEMWE cathodes,[2] but the scarcity and the high price of this metal calls for alternative catalysts based on earth-abundant elements.[3]

Molybdenum disulfide (MoS_2) has been identified as a promising material to electrocatalyze the HER due to its high catalytic activity and its stability over a wide potential and pH range.[4,5] The MoS_2 structure consists of two-dimensional layered materials whose S−Mo−S layers are held together by van der Waals interactions and are separated by 6.5 Å (trigonal coordinated structure 2H). Each layer is composed of two hexagonal planes of sulfur (S) atoms and an intermediate hexagonal plane of molybdenum (Mo) atoms. MoS_2 slabs mainly exhibit two types of edges: Mo-terminated edge (M-edge) and S-terminated edge (S-edge).[6,7] By linearly correlating the HER activity with the density of edge sites on model gold (111)-supported MoS_2 nanoparticles, Hellstern et al. evidenced that M-terminated edges are the active sites for the HER.[8] Therefore, the first approach to enhance the catalytic performance of these materials consists in controlling

Received: November 4, 2022
Revised: December 22, 2022
Published: January 5, 2023

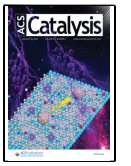

the morphology and the dispersion of the MoS_2 slabs (i.e., the HER activity per geometric surface area). Pushed to the limit, this strategy has led to the design of active $[Mo_3S_{13}]^{2-}$ clusters, although their stability is questionable.[8]

Another strategy to enhance the intrinsic HER activity of MoS_2 consists in using promoter metals.[9,10] Indeed, the addition of Co or nickel (Ni) promoters to the MoS_2 structure has been shown to enhance the catalytic activity for the widely studied hydrotreating reaction (HDT) by one order of magnitude.[11] The incorporation of promoter atoms takes place exclusively at the edges and modifies the S−metal bond energy, leading to a reduction of the S coverage on the active metal sites that weakens the H_{ads} binding energy.[12] On the other hand, faster HER kinetics has been reported of MoS_2 upon doping with single-metal atoms. For example, Zhang et al. reported enhanced HER performance through doping the basal plane of the MoS_2 slab with Ru single atoms, which they rationalized by combined synergistic effects of single-atom Ru doping and generation of S vacancies.[13] Similarly, other metals such as copper (Cu), Pt, and palladium (Pd) have been employed, and it was reported that doping metal integration boosts the catalytic performance through the activation of the basal plane.[10,14,15] However, active sites are located on the edges of MoS_2 and local atomic doping essentially takes place at the edges. For example, Weise et al. reported a catalyst with Pt integrated at the edges that resulted in substantially better HDT catalytic performance.[16] Consequently, the role of doping is still unclear.

The present work aims at disentangling whether the beneficial effect in activity is due to the doping itself or to an indirect effect impacting the density of edge sites by synthetically designing high-surface-area carbon-supported MoS_2 and Co−MoS_2 with a similar morphology, size, and dispersion. Besides Co, Ni, rhodium (Rh), Ir, and Pt−Co−MoS_2 trimetallic catalysts have been also reported to outperform Co−MoS_2 for the HDT.[16,17] Inspired by these studies and owing to the parallel existing between the HER and HDT, both reactions involving H adsorption, we thus extend our synthetic approach to Co−MoS_2/C doped with 1 wt % Pt ($Pt_{1\%}$−$CoMoS_2$/C).

2. EXPERIMENTAL SECTION

2.1. Catalysts Preparation. The three studied catalysts MoS_2/C, Co−MoS_2/C, and $Pt_{1\%}$−$CoMoS_2$/C were prepared by the incipient wetness impregnation method following a previously reported method.[18] The carbon black support (Vulcan XC 72 Cabot Corp., specific surface area of 223 m^2 g^{-1} and pore volume of 0.41 mL g^{-1}) was used as received. The aqueous impregnation solutions were prepared with a defined amount of ammonium heptamolybdate tetrahydrate [$(NH_4)_6Mo_7O_{24}{\cdot}4H_2O$, Merck] as well as a defined amount of citric acid ($C_6H_8O_7{\cdot}H_2O$, Prolabo) in order to obtain CA/(M) = 2 (M = Mo, Co, Pt). In previous work, we have shown that citric acid forms complex with Mo and thus decreases the rate of MoS_2 formation during the sulfidation step, leading to a small slab length. In this work, we took benefit from these findings by adjusting the amount of citric acid to the total molar concentration of the metal, but the variation was limited to achieve a constant pH of the impregnation solution.[18] For the Co-promoted MoS_2 sample, Co $(NO_3)_2{\cdot}_6H_2O$ (Alfa Aesar) was used with an atomic ratio equal to Co/Co + Mo = 0.3. For the $Pt_{1\%}$−$CoMoS_2$/C sample, ammonium hexachloroplatinate-(IV) [$(NH_4)_2PtCl_6$ Merck] was used. The content of Mo, Co was fixed to typical values used in representative industrial catalysts (11 wt % Mo, ∼3 wt % Co and 1 wt % Pt).[16] Finally, to obtain the catalyst in its sulfide form, a sulfidation procedure was performed at 623 K at a heating rate of 3 K min^{-1} at 0.1 MPa for 2 h under a 30 cm^3 min^{-1} flow of 10% H_2S/H_2.

2.2. HER Activity Measurements. Homogeneous catalytic inks were prepared by mixing the catalyst powder, a Nafion suspension (5 wt % in mixture of lower aliphatic alcohols and water), isopropanol, and ultrapure water (Millipore, 18.2 MΩ cm, total organic compounds < 3 ppb). An aliquot of this ink was then deposited onto the working electrode, a glassy carbon disk of 5 mm diameter. Then, Nafion and other solvents were evaporated. For the HER activity measurements, the catalyst loading was 300 μg_{powder} cm^{-2} for suldide-based materials and 20 μg_{Pt} cm^{-2} for the Pt/C reference material. All electrochemical measurements were carried out using a bipotentiostat (Autolab PGSTAT302N) operated with NOVA 2.0 software. All glassware used in this work was cleaned using a H_2SO_4/H_2O_2 (50% v/v) solution before use. We used a four-electrode electrochemical cell thermostated at T = 298 K. A carbon plate and a freshly prepared homemade reversible hydrogen electrode (RHE) were used as counter electrode and reference electrode, respectively. The electrochemical experiments were carried out using a rotating-disk electrode. For each sample, 10 HER cyclic voltammograms were recorded between 0.1 and −0.3 V versus the RHE at ν = 10 mV s^{-1} in an Ar-saturated 0.5 M H_2SO_4 electrolyte at 1600 rpm. The metric used to compare the different electrocatalysts was the value of the overpotential reported at a current density of 10 mA cm^{-2} (η_{10}). All electrochemical data were dynamically iR-corrected, where the solution resistance was determined by electrochemical impedance spectroscopy.

2.3. Microscopy Observation by High-Resolution Scanning Transmission Electron Microscopy−High-Angle Annular Dark Field (HR STEM-HAADF). The images of the catalysts after sulfidation were obtained using a double-corrected JEOL ARM 200F cold FEG microscope operated at 200 kV. The nanostructure and morphology of the MoS_2 and Co−MoS_2/C or $Pt_{1\%}$−$CoMoS_2$/C slabs were analyzed by high-resolution scanning transmission electron microscopy (HR STEM) using a high-angle annular dark field (HAADF) detector. The particle length was considered as the longest distance measured in each particle. The length distributions of sulfide slabs were determined statistically by measuring at least 100 slabs per sample. Only those particles that present 2H symmetry are considered, that is, isolated atoms or groups of few atoms for which it cannot be concluded if they correspond to the MoS_2 phase (present in a very low fraction) have been excluded. The image treatment was performed using the commercial software GMS3 from GATAN Inc. DigitalMicrograph. The average length ($\overline{L}$) was calculated according to the previous methodology described in refs 19 and 20.

2.4. MoS_2 Phase Characterization: X-ray Diffraction and Raman Spectroscopy. The powder X-ray diffraction (XRD) patterns were obtained on an XPERT-PRO diffractometer (Cu α radiation λ = 1.5401 angströms) in the 2θ range of 5−75° at a scanning rate of 1° min^{-1}, analyzing the samples in their sulfide form. Raman spectroscopy was performed on the sulfide catalysts using a Jobin Yvon LabRAM 300 Raman spectrometer equipped with a confocal microscope, a Nd-YAG laser (λ = 532 nm), and a charge-coupled device detector.

2.5. Inductively Coupled Plasma Mass Spectroscopy Coupled to an Electrochemical Flow Cell (FC-ICP-MS).

https://doi.org/10.1021/acscatal.2c05432
ACS Catal. 2023, 13, 1221−1229

The metal ions (^{94}Mo, ^{59}Co, and ^{195}Pt) were detected online with a PerkinElmer NexION 2000c inductively coupled plasma mass spectrometer coupled with a homemade electrochemical flow cell. These analyses are referred to as in situ flow cell−inductively coupled plasma mass spectroscopy (FC−ICP−MS) measurements in the work. Prior to the in situ FC−ICP−MS measurements, calibration curves were determined with daily prepared calibration solutions of ^{94}Mo, ^{59}Co, and ^{195}Pt at 0, 5, 10, and 20 μg L^{-1}. We used standard solutions (Carl Roth Gmbh & Co.) diluted with 0.05 mol L^{-1} H_2SO_4 (Suprapur 96%, Merck) in ultrapure water (Milli-Q, 18.2 MΩ cm, TOC < 3 ppb) for calibration. Calibrations were made before and after each FC−ICP−MS experiment to check the apparatus drift (<3%). A three-electrode configuration and an Autolab potentiostat (PGSTAT302N) were used for the FC−ICP−MS measurements. A commercial microelectrode Ag/AgCl/3.4 M Cl$^-$ (ET072, eDAQ) and a glassy carbon rod (SIGRADUR, HTW) were used as reference and counter electrode, respectively. The working electrode was a glassy carbon disk (5 mm diameter) embedded into a Teflon cylinder. The catalytic suspensions were prepared by mixing 16 mg of catalytic powder with 54 μL of a 5.0 wt % Nafion solution (Electrochem. Inc.), 1125 μL of isopropanol, and 700 μL of ultrapure water. 5 μL of the ultrasonically homogenized suspension was deposited into the working electrode, resulting in a catalyst loading of 20 μg_{Mo} cm^{-2}. The electrolyte consisted of a 0.05 mol L^{-1} H_2SO_4 solution deaerated with argon (Ar, 99.999%, Messer) and was pumped through the flow cell with a constant flow of 430 μL min^{-1} using a peristaltic pump. For metal detection, the flow cell outlet was connected to the ICP−MS nebulizer. The dwell time used was 100 ms with one replicate by reading. During the FC−ICP−MS measurements, the delay time between the Autolab and the ICP−MS signal was experimentally synchronized. Practically speaking, one potential pulse was applied, resulting in high-intensity ICP−MS signal and providing the response time (usually inferior to 4 s).

Twenty cyclic voltammograms between 0.1 and −0.2 V versus the RHE at v = 10 mV s^{-1} were performed. The experiments were conducted at room temperature (T = 295 + 2 K°), and all potentials are referred to the RHE. All in situ FC−ICP−MS measurements were performed at least two times, and the average values of the metal dissolution are shown. Error bars correspond to the standard deviation.

3. RESULTS AND DISCUSSION

3.1. 2H MoS_2 Phase Characterization. Figure 1a shows the XRD patterns of the three synthesized MoS_2 catalysts. The broad peaks detected are evidence of small crystallite size; nevertheless, it is possible to observe reflections that correspond to the MoS_2 hexagonal structure (molybdenite, ICSD card no. 98-002-1880). The two bands centered at 379 (E^1_{2g} mode) and 403 (A_{1g} mode) cm^{-1} characteristic of a hexagonal MoS_2 symmetry provide further evidence that the 2H structure of MoS_2 was synthesized (Figure 1b).

3.2. HR STEM-HAADF Characterization of MoS_2-Based Catalysts. Figure 2 shows the representative STEM-HAADF images with atomic resolution to get insights into the morphology of the MoS_2/C, Co−MoS_2/C, and $Pt_{1\%}$−$CoMoS_2$/C catalysts. The typical morphology of the three catalysts consists of extended MoS_2 plates, as previously observed for Al_2O_3-supported catalysts.[20] The formation of the thermodynamically stable trigonal prismatic 2H MoS_2 lattice

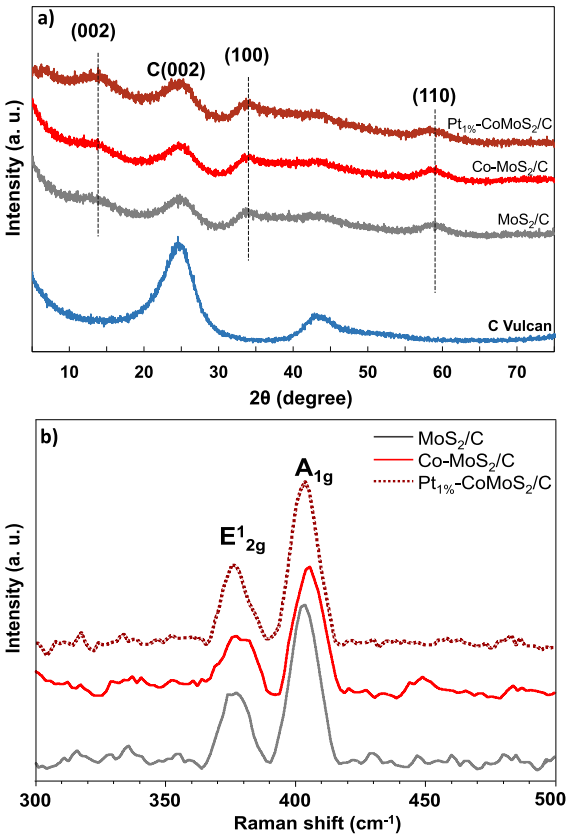

Figure 1. Structural characterization of the 2H MoS_2 phase. (a) XRD patterns of MoS_2/C, Co−MoS_2/C, and $Pt_{1\%}$−$CoMoS_2$/C and of the high-surface-area carbon support (Vulcan XC 72) used as a support. (b) Raman spectra of MoS_2/C, Co−MoS_2/C, and $Pt_{1\%}$−$CoMoS_2$/C supported on carbon catalysts showing the corresponding signals of the 2H−MoS_2 structure.

structure is revealed by the typical separation of about 0.63 nm detected on stacked slabs.[21] When observed in detail with greater magnification, it appears that the plates consist of very tiny particles with a mean size of 1.4 ± 0.2 nm for MoS_2, 1.4 ± 0.2 nm for Co−MoS_2/C, and 1.5 ± 0.2 nm for $Pt_{1\%}$−$CoMoS_2$/C. These small mean lengths are in line with the observed broad diffraction peaks (Figure 1a). Note that these values were obtained by measuring the longest transverse distance detected in the particle from the enhanced contrast HAADF images rather than from traditional TEM images. Indeed, the TEM images feature a poor contrast between the carbon support and the MoS_2 slabs. Furthermore, the fringes of the carbon support can be confused with MoS_2 slabs, adding additional error in the estimation of the particle size. Hence, only advanced HAADF images allow to rigorously monitor the size and shape of sulfide materials supported on carbon. The formation of tiny single-layer particles of less than one nanometer as well as clusters of few atoms was also detected (Figure 2b,e,h). The obtained images evidenced that Co and Pt addition had neither changed the size nor the shape of the slabs. In HAADF mode, the intensities of the contrast are directly proportional to the atomic number (Z) of the elements at the power 1.7,[7] leading to contrast variations between the Pt (Z = 78) and the Mo (Z = 42) or Co (Z = 27) atoms, as shown in Figures 2g,h. The atoms located in the bulk of the slabs present homogeneous brightness, while some of the atoms at the edges appear brighter, with intense contrast.

https://doi.org/10.1021/acscatal.2c05432
ACS Catal. 2023, 13, 1221−1229

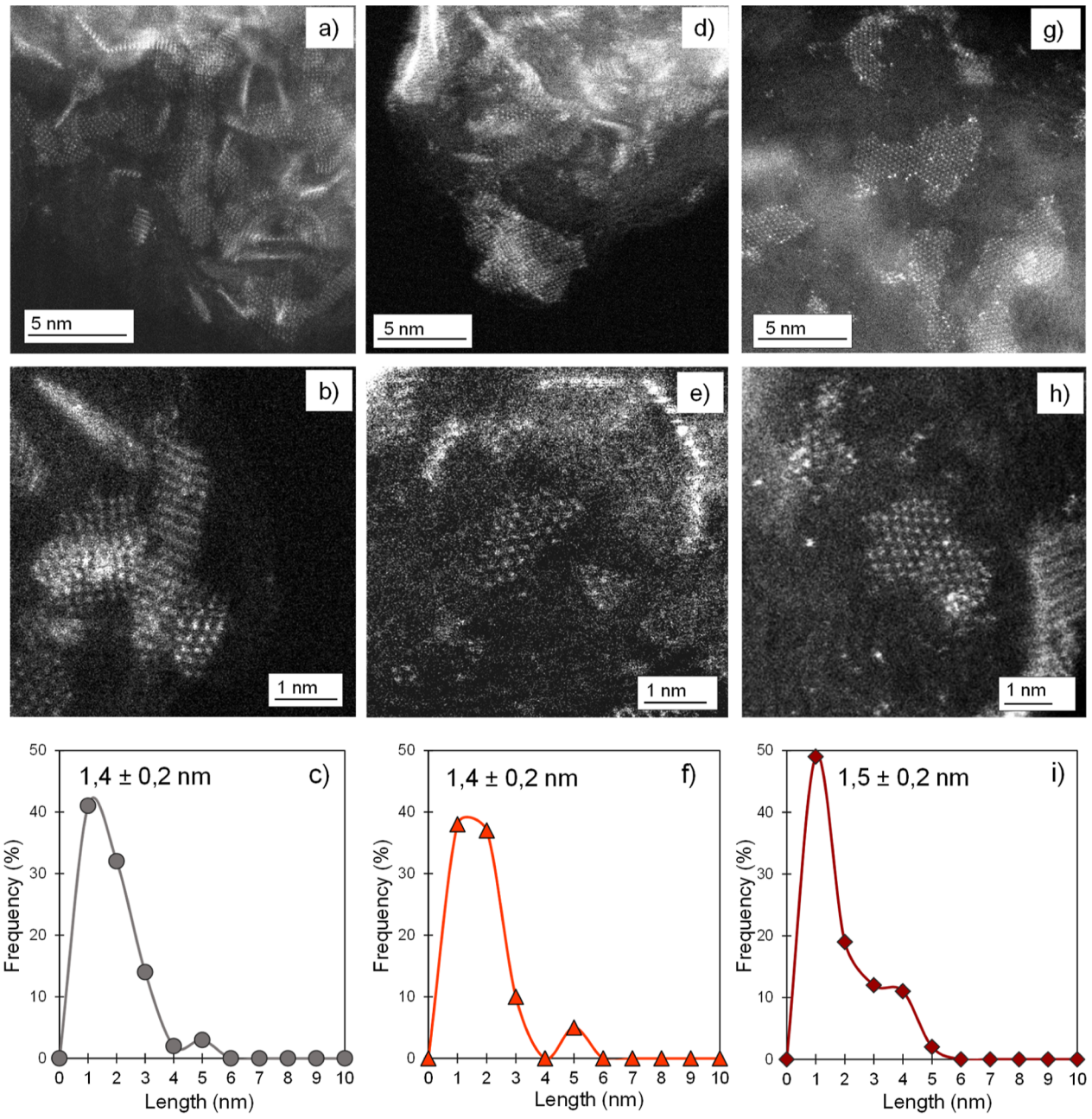

Figure 2. High-resolution STEM-HAADF micrographs of particles and length frequency histograms of (a–c) MoS_2/C, (d–f) Co–MoS_2/C, and (g–i) $Pt_{1\%}$–$CoMoS_2$/C catalysts.

These variations in contrast can be ascribed to Pt atoms being located at the edges, while Mo atoms are in the bulk, and they provide atomic-scale pieces of evidence of the promotion of the MoS_2 edges with Pt atoms. On the contrary, the location of Co atoms on the edges of the MoS_2 slab is not as easily observed by contrast variations despite the far difference in atomic numbers between Co and Mo atoms. This may be due to the depth variations typical of a material supported on a 3D architecture such as carbon black. Nevertheless, the improvement of the catalytic performance for HDT agrees with the decoration effect of Co, as previously reported for CoMoS slabs.[20]

3.3. HER Electrocatalytic Activity of Sulfide-Based Materials. Figure 3 displays the HER performance of the three MoS_2-based catalysts and of carbon black-supported Pt nanoparticles (Pt/C) as a reference. The best performance was observed for the commercial Pt/C catalyst and the MoS_2-based/C materials ranked as $Pt_{1\%}$–$CoMoS_2$/C > Co–MoS_2/C > MoS_2/C. The overpotential required to reach a geometrical current density of 10 mA cm^{-2} geo (η_{10}) was used as a metric to compare the HER activity of the MoS_2-based materials. An overpotential of 188 mV was reported for MoS_2/C, consistent with previous reports for nanostructured MoS_2, in particular for $[Mo_3S_{13}]^{2-}$ nanoclusters anchored on N-doped carbon nanotubes (Figure 3b).[22] Promotion by Co atoms at the edges of MoS_2 clusters led to a 48 mV decrease in the η_{10} value. Doping with single Pt atoms further decreased the η_{10} value by 22 mV, moving toward the performance of the reference Pt/C.[10,23] As the crystallite size, and thus the density of active sites, was identical for the three catalysts, we ascribed this

https://doi.org/10.1021/acscatal.2c05432
ACS Catal. 2023, 13, 1221–1229

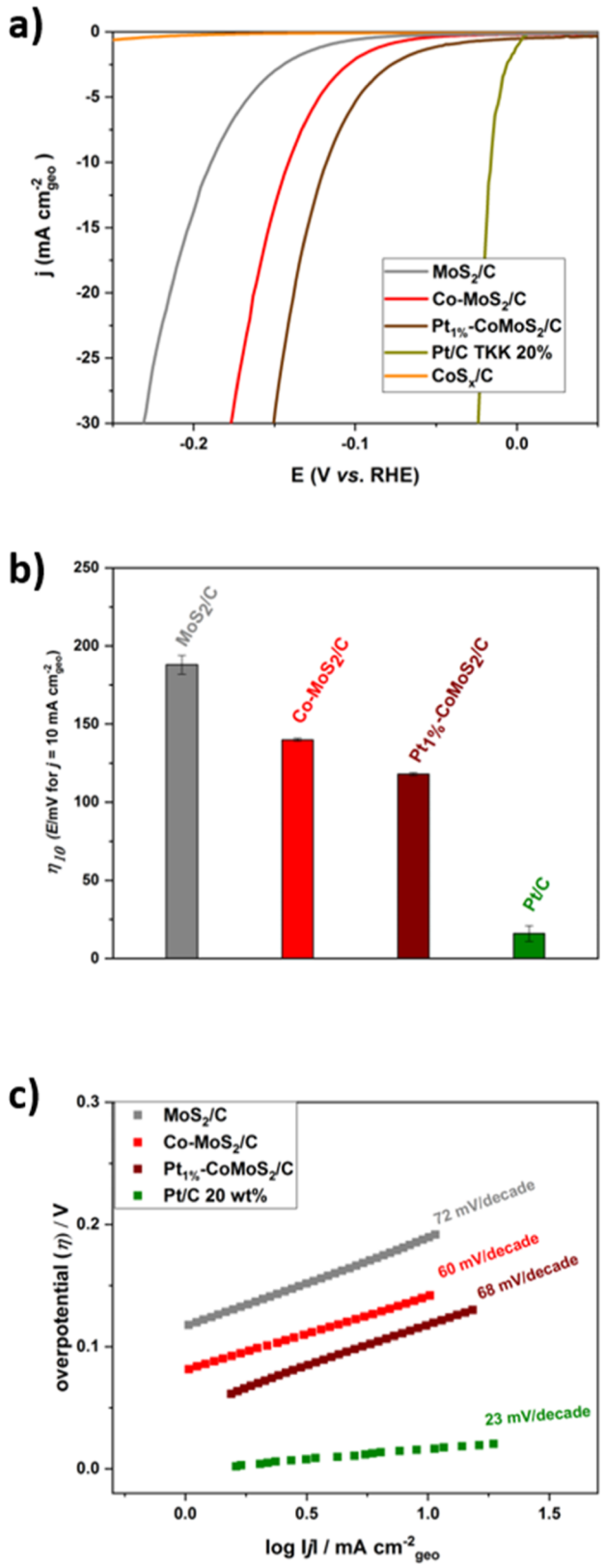

Figure 3. HER activity measurements. (a) Polarization curves, (b) overpotential measured at 10 mA cm^{-2} (η_{10}), and (c) Tafel plots for MoS_2/C, Co−MoS_2/C, Pt1%−$CoMoS_2$/C, and the commercial Pt/C reference catalysts. The HER polarization curves were measured in Ar-saturated 0.5 M H_2SO_4, ω = 1600 rpm, ν = 10 mV s^{-1}, and T = 298 K. The catalyst's loading was 300 μg_{powder} cm^{-2}.

performance to an electronic effect induced by the promoter Co and Pt atoms. Moreover, a cobalt sulfide supported on carbon black, CoS_x/C, synthesized using the same approach poorly performed toward the HER (Figure 1a, orange curve), confirming that the HER activity enhancement observed in Co−MoS_2/C is not due to added activities between two separated phases. Note also that Chia et al. have revealed that PtS_2 is active toward the HER in acidic media.[24] However, the overpotential required to reach a current density of 10 mA cm^{-2} amounts to 862 mV for the PtS_2 catalyst compared to 118 mV for $Pt_{1\%}$−$CoMoS_2$/C. The Tafel slope observed for the PtS_2 material is also 3 times higher (216 mV dec^{-1}) than that for $Pt_{1\%}$−$CoMoS_2$/C (68 mV dec^{-1}). For these reasons, should PtS_x species be formed during the synthesis, they would poorly contribute to the HER activity. Rather, we argue that the intimate contact between Co/Pt atoms and the MoS_2 slabs is responsible for HER activity enhancement. Our results evidence that Pt and Co doping enhances the HER activity, suggesting that different active sites may have formed. Evidence has been provided from the HDT reaction that Mo and S atoms located in the proximity of the Co atoms are involved in the catalytic cycle.[25] We thus propose that similar synergy takes place in the HER. Furthermore, as shown by DFT calculations, Co doping can lead to the activation of S_{edge} for H adsorption as H binding energy is decreased on these sites.[26] To gain insights into the HER mechanism, Tafel slopes were determined (Figure 3c). In acidic conditions, the HER is known to proceed according to three steps: (i) the adsorption of the first proton: $H_3O^+ + e^- \rightarrow H_{ads} + H_2O$ (Volmer step) followed by either (ii) the proton desorption $H_{ads} + H_3O^+ + e^- \rightarrow H_2 + H_2O$ (Heyrovsky step) or (iii) the recombination of two H_{ads} to form the H_2 molecule $H_{ads} + H_{ads} \rightarrow H_2$ (Tafel step). The value of the Tafel slope depends on which of these three steps is rate-determining, and 120, 40, and 30 mV decade^{-1} are the theoretical values for limitation by Volmer, Heyrovsky, and Tafel step, respectively. On Pt/C, a value of 30 mV decade^{-1} indicates that the Tafel step is the rate-limiting step at low overpotentials.[27] Higher values of Tafel slopes measured on MoS_2-based catalysts suggest different rate-determining steps. Several factors can account for that: (i) a lower electronic conductivity due to the semiconducting nature of the 2H phase, (ii) a more sluggish discharge of H_3O^+ ions, or (ii) a more sluggish electrochemical desorption of H_{ads} atoms from the MoS_2 surface. Importantly, the Co−MoS_2/C phase synthesized in this study exhibits a lower Tafel slope compared to MoS_2/C: this actually suggests that Co atoms modify the H_{ads} binding energy, in line with the results of former DFT calculations.[26] This effect was less pronounced in the case of $Pt_{1\%}$−$CoMoS_2$/C. Moreover, in the HDT reaction, Co promotion is ascribed to the increase of S electron density (basicity) and thus to an increase in S−H formation, which could favor the activation of edge sites for the HER.

Discussing the HER activity in more detail, we emphasize that Luo et al. reported a very active MoS_2 doped with 1 wt % of Pd atoms in substitution of Mo atoms. The authors used the octahedral 1T MoS_2, which is intrinsically more active owing to its higher electronic conductivity and to its higher density of active sites (both the edges and the basal planes are reported to be active for the HER in the 1T phase).[15,28] Nevertheless, the 1T phase is metastable and prone to revert to the 2H phase, rendering this strategy not viable for practical PEMWE devices. In contrast, the synthesis method described in this study leads to thermodynamically stable hexagonal 2H MoS_2 materials, as

https://doi.org/10.1021/acscatal.2c05432
ACS Catal. 2023, 13, 1221−1229

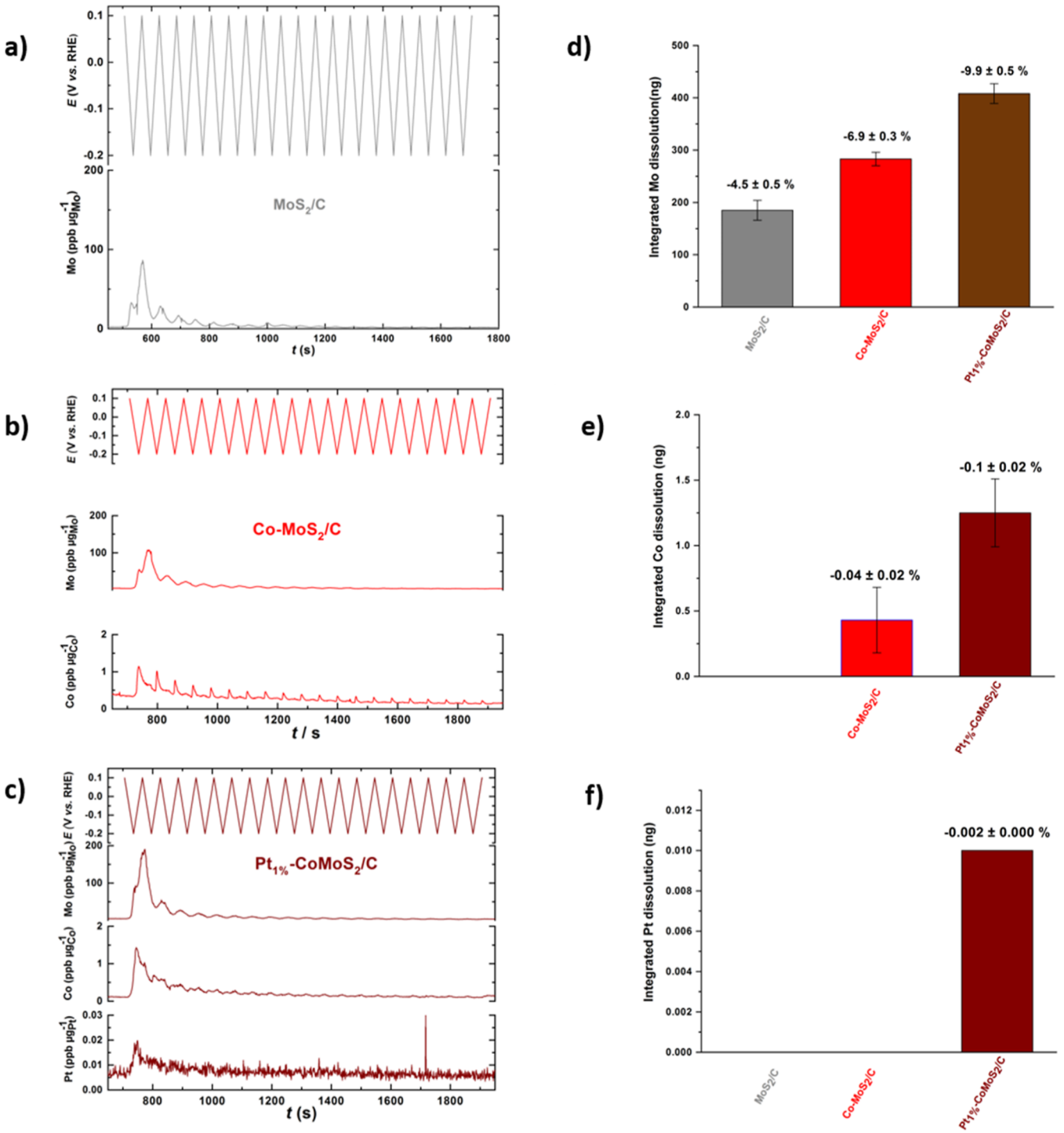

Figure 4. Stability of MoS_2-based electrocatalysts monitored by in situ FC−ICP−MS. Potential- and element-resolved dissolution measured during 20 HER cycles from −0.2 to 0.1 V vs the RHE at ν = 10 mV s^{-1} for (a) MoS_2/C, (b) Co−MoS_2/C, and (c) $Pt_{1\%}$−$CoMoS_2$/C. The quantities of dissolved elements during the protocol are presented in (d−f) for Mo, Co, and Pt, respectively.

confirmed by the diffraction patterns observed in XRD, by the stacking distance measured in STEM-HAADF images and by the two Raman peaks centered at 379 (E^1_{2g} mode) and 403 (A_{1g} mode) cm^{-1} characteristic of a hexagonal MoS_2 symmetry (Figure 1b). The alternative synthesis approaches described in this work thus demonstrate that it is possible to enhance the HER activity of the thermodynamically stable 2H phase of MoS_2 with only 1 wt % Pt.

Additional measurement comparing the HER performance of Pt/C and $Pt_{1\%}$−$CoMoS_2$/C at identical Pt loading has been performed and is displayed in Figure S2. Given the very low Tafel slope of Pt/C and its high intrinsic activity toward the HER, it was no surprise that Pt/C still remained far more active. It should be mentioned that Pt is in a very different state in the two electrodes: in the form of metallic Pt nanoparticles 2−3 nm in size in the commercial material versus single Pt atoms, promoting Mo−S edges of MoS_2 nanoclusters in $Pt_{1\%}$−

https://doi.org/10.1021/acscatal.2c05432
ACS Catal. 2023, 13, 1221−1229

$CoMoS_2$/C. Nevertheless, we can just infer that, from a practical point of view, Pt is largely underutilized when dispersed as single atoms onto the $Pt_{1\%}$−$CoMoS_2$/C catalyst as it acts as a doping element. In terms of pure HER performance, doping MoS_2 slabs with Pt is not a relevant strategy. However, this result is interesting from a fundamental point of view on the role of promoters. The choice of doping elements should be envisioned in the direction of non-noble metals.

3.4. In Situ Stability of MoS_2-Based Catalysts. To analytically assess the stability of the bare or doped MoS_2 nanocatalysts, the dissolution of Mo, Co, and Pt elements was monitored in situ using a flow cell connected to an inductively coupled mass spectrometer. Such a setup was introduced in our former study to dynamically monitor the dissolution of Ir, tin (Sn), and doping elements from IrO_x/doped-SnO_2 catalysts during the oxygen evolution reaction (OER).[29] We simulated the experimental conditions of a PEMWE cathode by applying a triangular cycling protocol between 0.1 and −0.2 V versus the RHE. Figure 4a−c displays the potential- and element-resolved dissolution for MoS_2/C, Co−MoS_2/C, and $Pt_{1\%}$−$CoMoS_2$/C, respectively. We first remark that elemental dissolution was always more pronounced during the first 3−5 potential cycles for Mo and for the doping elements. Note also that the scale in the *Y*-axis is different for Mo (0−200 ppb), Co (0−2 ppb), and Pt (0−0.02 ppb) elements. This difference suggests that most of dissolved Mo arise from oxysulfides, which were not entirely sulfidated during the sulfidation step (the presence of oxysulfides was already noticed in our former work; see ref 30). After these first potential cycles, the quantities of dissolved Mo, Pt, or Co decreased, approaching 1, <0.5, and <0.01 ppb, respectively. A closer look at the dissolution profiles shows that Mo, Co, and Pt dissolution initiates at −0.15 V versus the RHE during the anodic sweep, confirming that the doping elements were intimately linked together with the MoS_2 slabs. Interestingly, the calculated Pourbaix diagram of MoS_2 indicates that this potential corresponds to the transformation of MoS_2 into $[MoS_2]^{1-}$.[31] The presence of $[MoS_2]^{1-}$ thus surely facilitates the adsorption of the H_3O^+ ions on Mo sites but also seems to destabilize the MoS_2 structure. Further work is ongoing in our group to better understand these complex HER activity—durability relationships.

Finally, the quantities of Mo, Co, and Pt dissolved during the experiments were integrated and normalized to the amount initially loaded onto the backing electrode (Figure 4d−f). We found that at least 5% of the Mo atoms contained in the 2H MoS_2/C structures dissolved during the electrochemical protocol. In contrast, the quantities of dissolved promoters were extremely low: only 0.04 and 0.002% of the initial amount of Co and Pt were dissolved in the same conditions. Here again, we emphasize that the lack of stability essentially arises from partially sulfidated MoS_2/C, which dissolved during the first potential cycles. This hypothesis is supported by the much lower quantities of Mo, Co, and Pt dissolved in the last three cycles of the electrochemical protocol (Figure S1) showing less than 0.08% of Mo cumulatively dissolved. This result is in line with the former findings of Ledendecker et al. who reported more pronounced dissolution for Mo compared to MoS_2 during potential steps from the open-circuit voltage to −0.5 mA cm^{-2}.[32]

Another interesting point is related to the interplay between activity and stability. Indeed, similar to what was found for Ir-based catalysts for the OER, the most active electrocatalysts are the least stable.[33] Quantitively speaking, more Mo leached out from the bi- and trimetallic doped catalysts, which are more active for the HER compared to the bare MoS_2/C. The same holds true for Co as 0.04% of Co was dissolved from Co−MoS_2/C; this quantity is more than twice lower than for the more active Pt−$CoMoS_2$. This relationship confirms the link between HER activity (and the formation of $[MoS_2]^{1-}$ for the adsorption of the first proton) and dissolution keeping in mind that in the present experiments, the lower potential limit was similar for each catalyst. Further work will be performed to evaluate metal dissolution in potentiostatic conditions.

4. CONCLUSIONS

In conclusion, MoS_2/C-promoted Co−MoS_2/C and $Pt_{1\%}$−$CoMoS_2$/C nanoclusters were synthesized by an original incipient wetness impregnation method. The addition of a chelating agent in the synthesis protocol allowed us to control the crystallite size and thus the density of active sites. A similar morphology and structure (2H phase) were obtained for the mono-, bi-, and trimetallic sulfide catalysts. Doping with Co resulted in a 40 mV decrease of the overpotential at 10 mA cm^{-2} geo (η_{10}), confirming that substituting the edge Mo atoms of the 2H MoS_2 slabs with only 2−3 wt % of Co is a promising route to enhance the HER activity of MoS_2. $Pt_{1\%}$−$CoMoS_2$/C combines the beneficial effects of Co and Pt doping to further reduce the η_{10} value. However, at a similar Pt loading on the electrode, Pt/C nanoparticles best perform toward the HER. Since the crystallite size, the structure, and the density of active sites of the doped and undoped MoS_2/C catalysts are similar, the improved HER activity is attributed to the weakening of the H_{ads} binding energy via an electronic effect. Moreover, the in situ dissolution experiments revealed that doping/promoting with metal is a sustainable route according to the very low amount of Co and Pt dissolved under HER conditions.

■ ASSOCIATED CONTENT

Supporting Information

The Supporting Information is available free of charge at https://pubs.acs.org/doi/10.1021/acscatal.2c05432.

Stability of MoS_2-based electrocatalysts monitored by online FC−ICP−MS (PDF)

■ AUTHOR INFORMATION

Corresponding Authors

Laetitia Oliviero − *Laboratoire Catalyse et Spectrochimie, Normandie Université, ENSICAEN, UNICAEN, 14050 Caen, France*; orcid.org/0000-0002-7931-439X; Email: laetitia.oliviero@ensicaen.fr

Laetitia Dubau − *Université Grenoble Alpes, CNRS, Grenoble INP, Université Savoie Mont Blanc, LEPMI, 38000 Grenoble, France*; orcid.org/0000-0001-9520-1435; Email: laetitia.dubau@grenoble-inp.fr

Authors

Luz A. Zavala − *Laboratoire Catalyse et Spectrochimie, Normandie Université, ENSICAEN, UNICAEN, 14050 Caen, France*

Kavita Kumar − *Université Grenoble Alpes, CNRS, Grenoble INP, Université Savoie Mont Blanc, LEPMI, 38000 Grenoble, France*; orcid.org/0000-0003-3844-1082

https://doi.org/10.1021/acscatal.2c05432
ACS Catal. 2023, 13, 1221−1229

Vincent Martin − *Université Grenoble Alpes, CNRS, Grenoble INP, Université Savoie Mont Blanc, LEPMI, 38000 Grenoble, France*
Frédéric Maillard − *Université Grenoble Alpes, CNRS, Grenoble INP, Université Savoie Mont Blanc, LEPMI, 38000 Grenoble, France;* orcid.org/0000-0002-6470-8900
Françoise Maugé − *Laboratoire Catalyse et Spectrochimie, Normandie Université, ENSICAEN, UNICAEN, 14050 Caen, France*
Xavier Portier − *Centre de recherche sur les Ions, les Matériaux et la Photonique, CEA, UMR CNRS 6252, Normandie Université, ENSICAEN, UNICAEN, CNRS, 14050 Caen, France*

Complete contact information is available at: https://pubs.acs.org/10.1021/acscatal.2c05432

Author Contributions

The manuscript was written through the contributions of all authors. All authors have given approval to the final version of the manuscript. L.A.Z.: investigation, visualization, writing-original draft preparation, V.M.: investigation, methodology, writing−review, F.M.: investigation, methodology, writing−review, X.P.: investigation, methodology, writing−review, F.M.: writing−review, supervision, K.K.: investigation, methodology, writing−review, L.O.: methodology, writing−review, and editing, funding acquisition, supervision, L.D.: methodology, writing−review, and editing, funding acquisition, and supervision.

Notes

The authors declare no competing financial interest.

■ ACKNOWLEDGMENTS

The authors acknowledge the financial support of ANR CARNOT Energie et Systèmes de Propulsion (ESP) and ANR CARNOT Energies du Futur (EF) through the HERMOS project.

■ REFERENCES

(1) Wang, J.; Hu, C.; Shi, L.; Tian, N.; Huang, H.; Ou, H.; Zhang, Y. Energy and Environmental Catalysis Driven by Stress and Temperature-Variation. *J. Mater. Chem. A* **2021**, *9*, 12400−12432.
(2) Dubau, L.; Asset, T.; Chattot, V.; Bonnaud, J.; Vanpeene, V.; Nelayah, J.; Maillard, F. Tuning the Performance and the Stability of Porous Hollow PtNi/C Nanostructures for the Oxygen Reduction Reaction. *ACS Catal.* **2015**, *5*, 5333−5341.
(3) Asset, T.; Job, N.; Busby, Y.; Crisci, A.; Martin, V.; Stergiopoulos, V.; Bonnaud, C.; Serov, A.; Atanassov, P.; Chattot, R.; Dubau, L.; Maillard, F. Porous Hollow PtNi/C Electrocatalysts: Carbon Support Considerations to Meet Performance and Stability Requirements. *ACS Catal.* **2018**, *8*, 893−903.
(4) Benck, J. D.; Hellstern, T. R.; Kibsgaard, J.; Chakthranont, P.; Jaramillo, T. F. Catalyzing the Hydrogen Evolution Reaction (HER) with Molybdenum Sulfide Nanomaterials. *ACS Catal.* **2014**, *4*, 3957−3971.
(5) Hua, W.; Sun, H.; Xu, F.; Wang, J. A Review and Perspective on Molybdenum-Based Electrocatalysts for Hydrogen Evolution Reaction. *Rare Met.* **2020**, *39*, 335−351.
(6) Raybaud, P.; Hafner, J.; Kresse, G.; Kasztelan, S.; Toulhoat, H. *Ab Initio* Study of the H_2−H_2S/MoS_2 Gas—Solid Interface: The Nature of the Catalytically Active Sites. *J. Catal.* **2000**, *189*, 129−146.
(7) Chen, J.; Maugé, F.; El Fallah, J.; Oliviero, L. IR Spectroscopy Evidence of MoS_2 Morphology Change by Citric Acid Addition on MoS_2/Al_2O_3 Catalysts—A Step Forward to Differentiate the Reactivity of M-Edge and S-Edge. *J. Catal.* **2014**, *320*, 170−179.
(8) Hellstern, T. R.; Kibsgaard, J.; Tsai, C.; Palm, D. W.; King, L. A.; Abild-Pedersen, F.; Jaramillo, T. F. Investigating Catalyst-Support Interactions to Improve the Hydrogen Evolution Reaction Activity of Thiomolybdate $[Mo_3S_{13}]^{2-}$ Nanoclusters. *ACS Catal.* **2017**, *7*, 7126−7130.
(9) Dai, X.; Du, K.; Li, Z.; Liu, M.; Ma, Y.; Sun, H.; Zhang, X.; Yang, Y. Co-Doped MoS_2 Nanosheets with the Dominant CoMoS Phase Coated on Carbon as an Excellent Electrocatalyst for Hydrogen Evolution. *ACS Appl. Mater. Interfaces* **2015**, *7*, 27242−27253.
(10) Deng, J.; Li, H.; Xiao, J.; Tu, Y.; Deng, D.; Yang, H.; Tian, H.; Li, J.; Ren, P.; Bao, X. Triggering the Electrocatalytic Hydrogen Evolution Activity of the Inert Two-Dimensional MoS_2 Surface via Single-Atom Metal Doping. *Energy Environ. Sci.* **2015**, *8*, 1594−1601.
(11) Topsøe, H.; Clausen, B. S.; Massoth, F. E. *Catalysis Science and Technology*; Anderson, J. R., Boudart, M., Eds.; Springer: Berlin, 1996.
(12) Raybaud, P.; Hafner, J.; Kresse, G.; Kasztelan, S.; Toulhoat, H. Structure, Energetics, and Electronic Properties of the Surface of a Promoted MoS_2 Catalyst: An *Ab Initio* Local Density Functional Study. *J. Catal.* **2000**, *190*, 128−143.
(13) Zhang, J.; Xu, X.; Yang, L.; Cheng, D.; Cao, D. Atom Ru Doping Induced Phase Transition of MoS_2 and S Vacancy for Hydrogen Evolution Reaction. *Small Methods* **2019**, *3*, 1900653.
(14) Ji, L.; Yan, P.; Zhu, C.; Ma, C.; Wu, W.; Wei, C.; Shen, Y.; Chu, S.; Wang, J.; Du, Y.; Chen, J.; Yang, X.; Xu, Q. One-Pot Synthesis of Porous 1T-Phase MoS_2 Integrated with Single-Atom Cu Doping for Enhancing Electrocatalytic Hydrogen Evolution Reaction. *Appl. Catal. B* **2019**, *251*, 87−93.
(15) Luo, Z.; Ouyang, Y.; Zhang, H.; Xiao, M.; Ge, J.; Jiang, Z.; Wang, J.; Tang, D.; Cao, X.; Liu, C.; Xing, W. Chemically Activating MoS_2 via Spontaneous Atomic Palladium Interfacial Doping towards Efficient Hydrogen Evolution. *Nat. Commun.* **2018**, *9*, 2120.
(16) Weise, C. F.; Falsig, H.; Moses, P. G.; Helveg, S.; Brorson, M.; Hansen, L. P. Single-Atom Pt Promotion of Industrial Co−Mo−S Catalysts for Ultra-Deep Hydrodesulfurization. *J. Catal.* **2021**, *403*, 74−86.
(17) Pessayre, S.; Geantet, C.; Bacaud, R.; Vrinat, M.; Guyen, T. S. N.; Soldo, Y.; Hazemann, J. L. Platinum Doped Hydrotreating Catalysts for Deep Hydrodesulfurization of Diesel Fuels. *Ind. Eng. Chem. Res.* **2007**, *46*, 3877−3883.
(18) Chen, J.; Mi, J.; Li, K.; Wang, X.; Dominguez Garcia, E.; Cao, Y.; Jiang, L.; Oliviero, L.; Maugé, F. Role of Citric Acid in Preparing Highly Active CoMo/Al_2O_3 Catalyst: From Aqueous Impregnation Solution to Active Site Formation. *Ind. Eng. Chem. Res.* **2017**, *56*, 14172−14181.
(19) Zavala-Sanchez, L. A.; Portier, X.; Maugé, F.; Oliviero, L. Promoter Location on NiW/Al_2O_3Sulfide Catalysts: Parallel Study by IR/CO Spectroscopy and High-Resolution STEM-HAADF Microscopy. *ACS Catal.* **2020**, *10*, 6568−6578.
(20) Zavala-Sanchez, L.; Portier, X.; Maugé, F.; Oliviero, L. Formation and Stability of CoMoS Nanoclusters by the Addition of Citric Acid: A Study by High Resolution STEM-HAADF Microscopy. *Catal. Today* **2021**, *377*, 127−134.
(21) Xu, D.; Zhu, Y.; Liu, J.; Li, Y.; Peng, W.; Zhang, G.; Zhang, F.; Fan, X. Microwave-Assisted 1T to 2H Phase Reversion of MoS_2 in Solution: A Fast Route to Processable Dispersions of 2H-MoS_2 Nanosheets and Nanocomposites. *Nanotechnology* **2016**, *27*, 385604.
(22) Holzapfel, P. K. R.; Bühler, M.; Escalera-López, D.; Bierling, M.; Speck, F. D.; Mayrhofer, K. J. J.; Cherevko, S.; Pham, C. V.; Thiele, S. Fabrication of a Robust PEM Water Electrolyzer Based on Non-Noble Metal Cathode Catalyst: $[Mo_3S_{13}]^{2-}$ Clusters Anchored to N-Doped Carbon Nanotubes. *Small* **2020**, *16*, 2003161.
(23) Ye, J.; Chen, W.; Xu, S.; Yu, Z.; Hou, S. Synthesis of Co-Doped MoS_2/Graphene Hybrids as an Enhanced Electrocatalyst for Hydrogen Evolution Reaction. *RSC Adv.* **2016**, *6*, 104925−104932.
(24) Chia, X.; Adriano, A.; Lazar, P.; Sofer, Z.; Luxa, J.; Pumera, M. Layered Platinum Dichalcogenides (PtS_2, $PtSe_2$, and $PtTe_2$) Electrocatalysis: Monotonic Dependence on the Chalcogen Size. *Adv. Funct. Mater.* **2016**, *26*, 4306−4318.

(25) Mijoin, J.; Pérot, G.; Bataille, F.; Lemberton, J. L.; Breysse, M.; Kasztelan, S. Mechanistic Considerations on the Involvement of Dihydrointermediates in the Hydrodesulfurization of Dibenzothiophene-Type Compounds over Molybdenum Sulfide Catalysts. *Catal. Lett.* **2001**, *71*, 139−145.
(26) Russell, J.; Moses, P. G.; Jaramillo, T. F.; Nørskovb, J. K.; Chorkendorff, I. Hydrogen Evolution on Nano-Particulate Transition Metal Sulfide. *Faraday Discuss.* **2008**, *140*, 9−10.
(27) Conway, B. E.; Tilak, B. V. Interfacial Processes Involving Electrocatalytic Evolution and Oxidation of H_2, and the Role of Chemisorbed H. *Electrochim. Acta* **2002**, *47*, 3571−3594.
(28) Liu, Q.; Fang, Q.; Chu, W.; Wan, Y.; Li, X.; Xu, W.; Habib, M.; Tao, S.; Zhou, Y.; Liu, D.; Xiang, T.; Khalil, A.; Wu, X.; Chhowalla, M.; Ajayan, P. M.; Song, L. Electron-Doped 1T-MoS_2 via Interface Engineering for Enhanced Electrocatalytic Hydrogen Evolution. *Chem. Mater.* **2017**, *29*, 4738−4744.
(29) Abbou, S.; Chattot, R.; Martin, V.; Claudel, F.; Solà-Hernandez, L.; Beauger, C.; Dubau, L.; Maillard, F. Manipulating the Corrosion Resistance of SnO_2 Aerogels through Doping for Efficient and Durable Oxygen Evolution Reaction Electrocatalysis in Acidic Media. *ACS Catal.* **2020**, *10*, 7283−7294.
(30) Oliviero, L.; Travert, A.; Dominguez Garcia, E.; Chen, J.; Maugé, F. Catalysis by Sulfides: Advanced IR/CO Spectroscopy for the Identification of the Most Active Sites in Hydrodesulfurization Reactions. *J. Catal.* **2021**, *403*, 87−97.
(31) Huang, Y.; Nielsen, R. J.; Goddard, W. A.; Soriaga, M. P. The Reaction Mechanism with Free Energy Barriers for Electrochemical Dihydrogen Evolution on MoS_2. *J. Am. Chem. Soc.* **2015**, *137*, 6692−6698.
(32) Ledendecker, M.; Mondschein, J. S.; Kasian, O.; Geiger, S.; Göhl, D.; Schalenbach, M.; Zeradjanin, A.; Cherevko, S.; Schaak, R. E.; Mayrhofer, K. Stability and Activity of Non-Noble-Metal-Based Catalysts Toward the Hydrogen Evolution Reaction. *Angew. Chem., Int. Ed.* **2017**, *56*, 9767−9771.
(33) Daiane Ferreira da Silva, C.; Claudel, F.; Martin, V.; Chattot, R.; et al. Oxygen Evolution Reaction Activity and Stability Benchmarks for Supported and Unsupported IrO_x Electrocatalysts. *ACS Catal.* **2021**, *11*, 4107−4116.

https://doi.org/10.1021/acscatal.2c05432
ACS Catal. 2023, 13, 1221−1229